




Mechanical Characterization of 3D Ovarian Cancer Nodules Using Brillouin Confocal Microscopy

CHRISTINA CONRAD,¹ KELSEY M. GRAY,¹ KIMBERLY M. STROKA,¹ IMRAN RIZVI,²
and GIULIANO SCARCELLI ¹

¹Fischell Department of Bioengineering, University of Maryland, 4228 A. James Clark Hall, College Park, MD 20742, USA; and
²Joint Department of Biomedical Engineering, University of North Carolina at Chapel Hill and North Carolina State University,
Chapel Hill, NC 27599, USA

(Received 2 December 2018; accepted 13 April 2019; published online 7 May 2019)

Associate Editor James L. McGrath oversaw the review of this article.

Abstract

Introduction—The mechanical interaction between cells and their microenvironment is emerging as an important determinant of cancer progression and sensitivity to treatment, including in ovarian cancer (OvCa). However, current technologies limit mechanical analysis in 3D culture systems. Brillouin Confocal Microscopy is an optical non-contact method to assess the mechanical properties of biological materials. Here, we validate the ability of this technology to assess the mechanical properties of 3D tumor nodules.

Methods—OvCa cells were cultured in 3D using two established methods: (1) overlay cultures on Matrigel; (2) spheroids in ultra-low attachment plates. To alter the mechanical state of these tumors, nodules were immersed in PBS with varying levels of sucrose to induce osmotic stress. Next, nodule mechanical properties were measured by Brillouin microscopy and validated with standard stress–strain tests: Atomic Force Microscopy (AFM) and a parallel plate compression device (Microsquisher). Finally, the nodules were treated with a chemotherapeutic commonly used to manage OvCa, carboplatin, to determine treatment-induced effects on tumor mechanical properties.

Results—Brillouin microscopy allows mechanical analysis with limited penetration depth (~92 μm for Matrigel method; ~54 μm for low attachment method). Brillouin microscopy metrics displayed the same trends as the corresponding “gold-standard” Young’s moduli measured with stress–strain methods when the osmolality of the medium was increased. Nodules treated with carboplatin showed a decrease in Brillouin frequency shift.

Conclusion—This validation study paves the way to evaluate the mechanics of 3D nodules, with micron-scale three-

dimensional resolution and without contact, thus extending the experimental possibilities.

Keywords—Tumors, Osmolality, Young’s modulus, Stiffness, Spheroids, Optics, Atomic force microscopy, MicroSquisher.

INTRODUCTION

Improvements in outcomes for advanced stage ovarian cancer (OvCa) continue to lag behind many other solid tumors with a 5-year survival rate of 45%, which is further reduced to 31% after 10 years.^{8,25,36,43} OvCa is often referred to as a ‘silent killer’ because the symptoms often remain unremarkable until late stages.¹³ OvCa etiology is not well established; there are five known histotypes: high-grade serous, endometrioid, clear cell, mucinous, and low-grade serous, all which differ in pathology, site of origin, and behavior.³⁵ Furthermore, cell populations exhibit heterogeneity with varying levels of proliferation, invasiveness and resistance to chemotherapy.^{4,7,20,32,36,46} In recent years, a relationship between OvCa aggressiveness and mechanical properties was observed, providing evidence that mechanical adaptation contributes to cell migration and survival. For instance, several groups have shown that highly malignant OvCa cells have lower Young’s moduli compared to benign cells using mechanical testing systems including atomic force microscopy (AFM) and magnetic tweezers.^{11,22,44,52} Mechanical variations are also related to changes in structural protein content; for example, increased metastatic potential has been correlated with decreased E-Cadherin, increased vimentin, and decreased actin.^{1,20,22,36,44,52} The role of

Address correspondence to Imran Rizvi, Joint Department of Biomedical Engineering, University of North Carolina at Chapel Hill and North Carolina State University, Chapel Hill, NC 27599, USA; Giuliano Scarcelli, Fischell Department of Bioengineering, University of Maryland, 4228 A. James Clark Hall, College Park, MD 20742, USA. Electronic mails: imran.rizvi@unc.edu, scarcel@umd.edu

Imran Rizvi and Giuliano Scarcelli have contributed equally to this work.

the mechanical properties of cancer cells and tissues has attracted much interest in recent years, even leading to the idea to generate novel therapeutics based on the mechanical regulation of cells or their microenvironment.^{30,32}

It is widely accepted that cells sense and respond to mechanical cues in their microenvironment; however, the underlying causes of mechanical changes and the implications of altered mechanical properties in cancer progression remain areas of continued investigation.^{1,12,19,24,28–30,33,34,45,49,53} A largely underestimated regulator of mechanical properties is osmotic pressure of the extracellular environment. On short time scales, i.e., immediately after adding the solute, changes in mechanical properties have been explained due to water efflux from cells and the resulting osmotic pressure gradient.^{17,31,40,55} In single cells, several groups have explored the effects of hyperosmotic stress and have shown a positive correlation with Young's modulus.^{17,31,40,55} Yet, single cells do not adequately portray disease pathology and many groups have sought to generate 3D tumors, organoids, or biomaterials to reflect mechanical and biochemical components of the microenvironment and thus investigate how cells respond to various environmental stimuli.^{3,15,24,29,33,36}

A major limitation of current technologies that measure the mechanical properties of biological samples is that they require contact with the sample and are severely limited in complex 3D matrix environments or other systems that do not offer direct access to cells. Therefore, a non-contact approach to extract the mechanical features of complex biological systems will be of value, particularly in cancer-related mechanobiology studies. One potential technology to address this need is Brillouin microscopy. Brillouin light scattering is a phenomenon where interaction of incident light with acoustic phonons within a material causes a frequency shift in the scattered radiation. The Brillouin frequency shift is related to the longitudinal modulus of the sample, i.e. the ratio of stress–strain in a purely uniaxial setting at high-frequency (GHz). Thus, combining a high-resolution Brillouin spectrometer with confocal microscopy, will enable three-dimensional maps of material mechanics to be generated.

Here, a human carcinoma cell line derived from intraperitoneal metastases (NIH: OVCAR5) was cultured as 3D tumor nodules using two methods: (1) overlay cultures on Matrigel (CorningTM); and (2) Spheroids in 96 Well Ultra-Low Attachment Microplates (CorningTM). Using Brillouin, we showed that increasing osmotic pressure in tumor nodules caused an increase in Brillouin shift. However, as biological cells and tissues are nearly incompressible and present large frequency-dependent changes, the relationship between Brillouin-derived longitudinal modulus and

traditional quasi-static Young's modulus is not known and relies on empirical correlations. Thus, we validated Brillouin Confocal Microscopy to assess 3D tumor nodule mechanical properties by comparing Brillouin frequency shift to Young's modulus measured with two gold-standard mechanical methods: AFM and a Micro-Scale Mechanical Tester (MicroSquisher). Previous relationships have been established in biological samples, including ocular tissue^{38,42,47} and single cells,⁴⁰ where a positive correlation to Young's modulus has been found. Likewise, we found an increase in Young's modulus upon increasing osmolality.

Next, we examined the effects of carboplatin treatment in tumor nodules using Brillouin Microscopy. Carboplatin is a common chemotherapeutic used to manage OvCa. Carboplatin triggers cell death (e.g. apoptosis) by forming DNA adducts, which interferes with DNA synthesis and inhibits DNA repair mechanisms.¹⁰ Nodules were grown using the overlay culture method on Matrigel for 7 days and given a strong (500 μ M) dose of carboplatin. Brillouin measurements after 96 h showed a decrease in overall Brillouin shift. From these results, we established an expected range of Brillouin shift for ovarian cancer tumor nodules; from high Brillouin shifts caused by hyperosmotic conditions to low Brillouin shifts caused by carboplatin. Using Brillouin microscopy, the mechanical properties of tumors can be mapped with high resolution without the need for contact or labeling, enabling unique experimental designs.

MATERIALS AND METHODS

Cell Culture

Epithelial ovarian cancer cells (NIH: OVCAR5) were grown in standard conditions using the recommended culture medium containing RPMI 1640 Medium, no phenol red, 10% Fetal Bovine Serum (FBS), and 1% Pen Strep.

Culture of Nodules Using Matrigel Overlay Method

Corning[®] Matrigel[®] (Growth Factor Reduced (GFR) Basement Membrane Matrix Phenol Red-Free, *LDEV-Free #356231) was used as the extracellular matrix for the cultures. Matrigel was thawed overnight on ice at 4 °C. The following day, 250 μ L of thawed Matrigel was pipetted into wells of a sterile glass bottom 24-well plate (Greiner bio-one Sensoplate, #662892). Matrigel was polymerized by incubating at 37 °C for 20 min. 1 mL of 10⁴ cells/mL OVCAR5 cells in medium supplemented with 2% Matrigel was added per well. Media was replaced every 3 days by gently aspirating old medium to not disturb nodules attached to the Matrigel.

Culture of Nodules Using Low Attachment Plates

Corning™ 96 Well Ultra-Low Attachment Treated Spheroid Microplates (Fisher Scientific, #12-456-721) provided a method for growing larger nodules without the need for Matrigel, favorable for the Microsquisher and AFM, where contact with the nodule is required and the presence of Matrigel could skew the results. To prepare nodules, 300 μL of OVCAR5 at a concentration of 10^5 cells/mL in OVCAR5 medium was added to 96 wells and incubated at 37 °C for 3 days. 12-mm glass coverslips coated in collagen were prepared to provide a surface for nodule attachment: Glass coverslips were initially sterilized with 70% ethanol. A composition Rat Tail Type I Collagen High protein concentration (Corning™, #354249, protein concentration: 10.21 mg/mL) and 70% ethanol at a 1:4 ratio was prepared. 50 μL of the mix was added per coverslip and stored overnight at room temperature. On day 3 of nodule growth, nodules were removed from the 96-well plate by slowly pipetting with a 10 mL pipette tip and transferred to collagen coated coverslips. Nodules were incubated in 37 °C for 24 h to provide time to attach.

Osmolality Measurements

Concentrations of sucrose up to 1000 mM in Phosphate Buffered Saline (PBS, Dulbecco's phosphate-buffered saline, 1 \times) was added to the extracellular fluid of nodules. A relationship between sucrose concentration and osmolality was established by measuring solutions with an Advanced® Micro-Osmometer Model 3300 (Table 1).

Brillouin Light Scattering

Brillouin light scattering (BLS) is based on the interaction between light and acoustic phonons within matter. Brillouin frequency shift (v_B) is related to the phonon velocity (V_s) by

$$v_B = \pm \frac{2nV_s}{\lambda} \sin \frac{\theta}{2} \quad (1)$$

where n is the refractive index, λ is the incident wavelength, and θ is the angle of the incident light. Here, we used a backscattering configuration, so the $\sin \frac{\theta}{2} \sim 1$. Furthermore, phonon velocity is related to the longitudinal Young's modulus and mass density (ρ) by $V_s = \sqrt{\frac{M'}{\rho}}$ where M' is the real part of the longitudinal modulus. Combining these equations, Brillouin frequency shift is related to longitudinal modulus as

$$v_B = \pm \frac{2n}{\lambda} \sqrt{\frac{M'}{\rho}} \quad (2)$$

The ratio $n/\sqrt{\rho}$ has been shown to vary insignificantly in cells and tissue therefore the frequency shift is directly related to longitudinal modulus.⁴⁰ For this work, we report Brillouin frequency shift (GHz) displayed by a color bar where warmer colors (red) correspond to an increase in Brillouin frequency shift and thus increase in longitudinal modulus.

Brillouin Confocal Microscopy

A single mode linearly-polarized continuous wave laser (Toros, Laser Quantum) with a wavelength of either 660 nm or 532 nm (for carboplatin experiments) was directed into an inverted microscope (Olympus IX81) where light was focused into the sample using a 60X/0.7 NA objective lens (Olympus, LUCPLFLN60X). Backwards scattered light was collected using the same objective lens and coupled into the Brillouin spectrometer comprised of two-stage VIPA etalons arranged in cross-axis configuration.^{40,54} A program created in-house (LabVIEW) provided control of translational stages (Prior) image acquisition (Andor), region of interest selection, scanning step size, and exposure time. The free spectral range (FSR) i.e. wavelength separation between adjacent identical stokes/anti-stokes peaks and GHz per pixel i.e. factor to convert image pixels to frequency were determined by calibrating with water and methanol which have known Brillouin shifts. For 3D imaging (Fig. 1d), we performed raster scanning in the XY dimension and refocused to a new location along the Z axis to generate another stacked image. For all other measurements (Figs. 2, 3, and 5), images were acquired in the central XZ plane perpendicular to the Matrigel bed. The spatial resolution of the images depends on the NA of the objective lens; here, the lateral resolution was 1 μm and axial resolution was 2 μm . A post-processing algorithm developed in MATLAB was used to fit the Brillouin peaks to a Lorentzian function and

TABLE 1. Relationship between osmolality and sucrose concentration in PBS measured by an osmometer.

Sucrose concentration (mM)	Measured osmolality (mOsm/kg H ₂ O)	
	Mean	Standard deviation
0	285	4.58
250	546	5.69
500	847	1.53
750	1141	11.50
1000	1440	8.39

extrapolate the average Brillouin frequency shift. Average nodule Brillouin frequency shift was determined by excluding the locations pertaining to the surrounding medium and averaging values corresponding to the remaining nodule structure.

The mechanical response of nodules cultured using Matrigel was tested under 3 osmotic conditions: 0, 500 mM, and 1000 mM sucrose. After 3 days of culture, 3 nodules in 3 separate wells, for a total of 9 nodules per condition were tested. Brillouin imaging was performed immediately after the addition of sucrose. Images were acquired in the XZ plane with 1 μm resolution. Due to the poor signal penetration depth in the z-direction for low attachment nodules, we imaged 100 \times 100 μm sections in the XY plane where the signal was resolvable with 2 μm resolution. Nodules cultured using the low attachment plates were subjected to 0, 62.5 mM, and 125 mM sucrose. The decreased osmotic condition was required due to decrease signal intensity in the low attachment nodules (Fig. 2c). A total of 6 nodules were measured per condition.

Young's Modulus Measured Using Atomic Force Microscopy

The Young's modulus was measured using an Asylum MFP-3D-BIO AFM with CP-qp-CONT-Au sphere colloidal probe (NanoAndMore USA Corp.) having a diameter of 3–5.5 μm according to the manufacturer. The spring constant of the cantilever was measured to be 0.17 N/m, which was within a factor of 1.69 to the manufacturer's nominal value of 0.1 N/m.

AFM was performed using a 3 μm force distance, a 1 V trigger point (\sim 8.7 to 8.8 nN), and a scan rate of 0.99 Hz. Force curves were fit to the Hertz model within Asylum's Igor Pro-based software, using the equation

$$F = \frac{4}{3} \times \frac{E}{1 - \nu^2} \times \sqrt{r} \times \delta^{3/2} \quad (3)$$

with δ as the measured indentation of the sample and Young's modulus E as the fitting parameter. The Poisson's ratio ν of the sample was assumed to be 0.45 and the tip radius of curvature r was approximately 2.1 μm .

OVCAR5 tumor nodules were cultured using the low attachment method and attached to collagen coated glass coverslips as previously described. Nodules were placed in a Falcon® 50 mm \times 9 mm Sterile Petri Dish (New Star Environmental and Laboratory Products #351006) and bathed in 4 mL of PBS with varying concentrations of sucrose (0, 500, and 1000 mM) warmed at 37 $^{\circ}\text{C}$. Three 10 \times 10 force maps spanning 2500 μm^2 (5 μm step size) were acquired per nodule and 3 nodules per sucrose level were tested.

Young's Modulus Measured Using MicroSquisher (Cell Scale)

Nodules were prepared using the low attachment protocol previous described. Nodules were placed in a fluid bath of PBS-sucrose solution warmed to 37 $^{\circ}\text{C}$. A total of 35 nodules were measured in varying sucrose conditions: 0, 250, 500, 750, and 1000 mM. A mi-

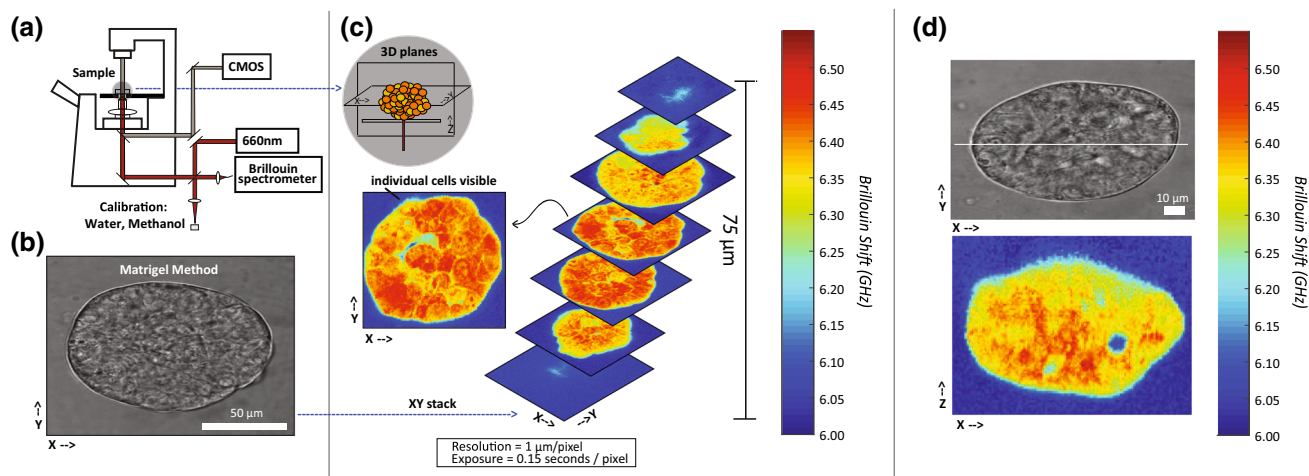


FIGURE 1. (a) Brillouin Confocal Microscope configuration. Light at 660 nm is focused onto the sample and back scattered light is collected by the same objective lens and directed to the Brillouin spectrometer. (b) Brightfield image of a nodule cultured on Matrigel. (c) Three-dimensional stacks of XY plane images of the nodule corresponding to (b). Color bar represents Brillouin shift in GHz, where increased Brillouin shift is related to increased longitudinal modulus. The resolution of the image was 1 μm per pixel and the exposure was 0.15 s per pixel. (d) An example Brillouin map and brightfield image of a nodule cultured using Matrigel measured in the XZ plane (perpendicular to the Matrigel surface).

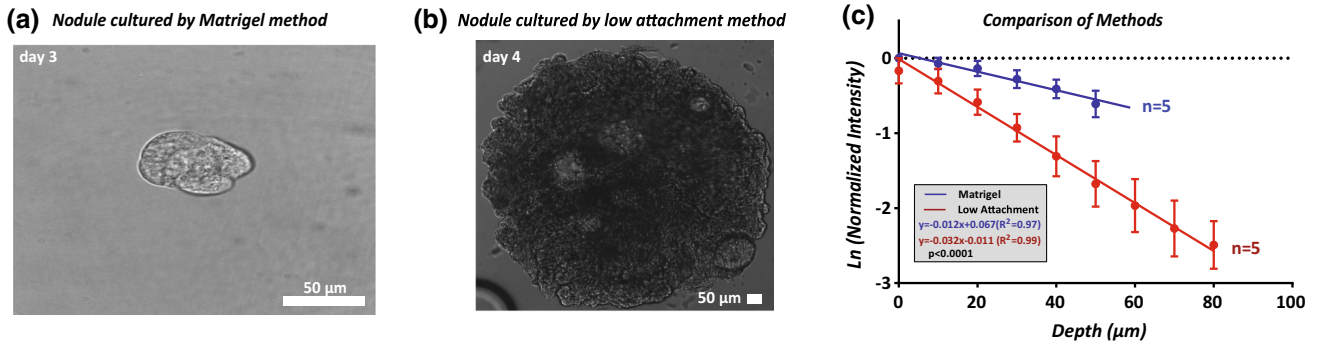


FIGURE 2. (a) Brightfield image (objective: $\times 60$) of nodules after 3 days of culture on Matrigel method. (b) Brightfield image (objective: $\times 10$) of nodule on day 4 cultured using the low attachment method. (c) Depth in the z axis (μm) vs. natural log of normalized intensity for Matrigel ($N = 5$) and low attachment ($N = 5$) nodules. A comparison of liner fits shows significant differences ($p \leq 0.0001$) between methods in signal decay.

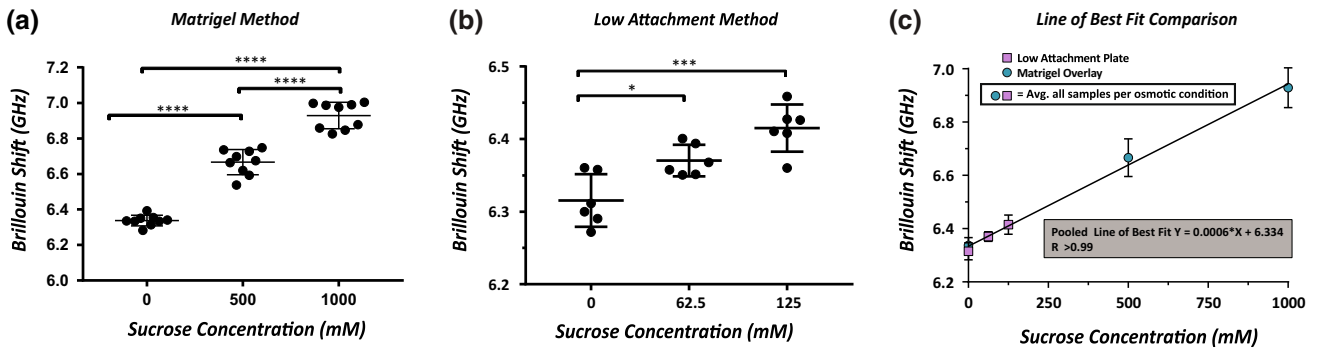


FIGURE 3. (a) Increased osmolality of extracellular solution for nodules cultured using Matrigel method caused an increased nodule Brillouin Shift. (b) Increased osmolality of nodules cultured by low attachment method caused increased Brillouin shift. (c) Low attachment method created larger nodules, Brillouin shift was directly dependent on osmolality of the PBS-sucrose solution. Nodules correlated with an increase in osmolality ($R^2 = 0.99$).

crobeam with a diameter of $152.4 \mu\text{m}$, modulus $411,000 \text{ MPa}$, and length of 60 mm was fixed to a $2 \times 2 \text{ mm}^2$ compression plate and mounted to the vertical actuator. Data acquisition was performed using the software provided, SquisherJoy. Nodules were compressed once in the Z-axis by ramping up to 75%, with a load time of 20 s, hold of 10 s, and recovery period of 20 s. Data was exported to Microsoft Excel where analysis was performed. The Young's modulus was calculated as the slope of the stress strain curve using the formula:

$$E = \frac{F/A}{\Delta L/L} \quad (4)$$

where E is the Young's modulus ($\mu\text{N}/\mu\text{m}^2$), F is the force in (μN), A is the surface area of the nodule (μm^2), L is the height of the nodule (μm), and ΔL is the displacement of the beam (μm). The surface area (A) was measured by assuming a circle as the shape of the surface. ImageJ was used to determine the diameter of the nodule at 10% strain.⁴¹ The length of the nodule (L) was gathered by the SquisherJoy software, where

cursor was placed prior to testing at the top and bottom of the nodule. The Young's modulus was analyzed between 0 and 10% strain where initial strain (0%) was assumed to be when the applied force reached $0.1 \mu\text{N}$. Culture methods for mechanical testing using Brillouin, AFM, and the Microsquisher are summarized in Table 2.

Carboplatin Treatments

OVCAR5 tumor nodules were cultured for 7 days using the protocol for forming nodules with Matrigel as previously described. Medium changes occurred on days 3 and 6 of culture. On day 7, nodules were dosed with $500 \mu\text{M}$ carboplatin in 1 mL of medium while non-treated groups were refreshed with 1 mL of medium. After 96 h of incubation in 37°C , the Brillouin shift of non-treated and treated cells were measured. To retrieve Brillouin shift of the nodules, the extracellular medium was removed by thresholding values less than 7.65 GHz and the Brillouin shift was average across the remaining area of the nodule. Experiments

TABLE 2. Summary of techniques and culture method, duration, conditions, and number of samples for mechanical analysis.

Methods summary				
Technique	Culture method	Culture duration (days)	Conditions (sucrose concentration mM)	Samples per condition
Brillouin	Matrigel	3	0, 500, 1000	9 nodules
Brillouin	Low attachment	4	0, 62.5, 125	6 nodules
AFM	Low attachment	4	0, 500, 1000	3 nodules (3 regions of interest per nodule)
Microsquisher	Low attachment	4	0, 250, 500, 750, 1000	8, 7, 7, 7, 6 nodules respectively

were performed using a previous set up which used a green laser ($\lambda = 532$ nm). Brillouin shifts using a green laser can be converted to red laser ($\lambda = 660$ nm) by multiplying by the ratio of wavelengths; Red Brillouin Shift = Green Brillouin Shift * (532/660). A total of 19 non-treated and 20 treated nodules were measured in three separate rounds.

Statistical Analysis

For osmotic pressure experiments, a one-way ANOVA was used to compare groups. For the carboplatin treatment experiment, a paired t test assuming equal variances was used to compare to the non-treatment group. All statistics were performed using GraphPad Prism7. * ≤ 0.05 ** ≤ 0.01 , *** ≤ 0.001 , **** ≤ 0.0001 .

RESULTS

Mechanical Mapping of Nodules Using Brillouin Confocal Microscopy

Figure 1 shows the Brillouin instrument setup and representative images of 3D OvCa nodules acquired with the Brillouin instrument. The Brillouin instrument is co-registered with a brightfield transmission microscope (Fig. 1a). A brightfield image of a tumor nodule after 5 days in culture using the Matrigel overlay method is shown in Fig. 1b. A series of corresponding Brillouin XY cross-sectional images, taken at $12.5 \mu\text{m}$ step along the Z depth axis, are shown in Fig. 1c and demonstrate the 3D sectioning capability provided by the confocal nature of Brillouin measurements. For the rest of the paper, to perform Brillouin imaging on a large population of nodules, we scanned one depth-section (XZ plane) per nodule; we chose the XZ plane cutting through the central axis of the nodule, to maintain consistency in the assessed location across measurements. An example brightfield image in the XY plane of a nodule cultured using the Matrigel method and corresponding Brillouin map in the XZ plane is shown in Fig. 1d. High resolution

Brillouin images revealed tumor nodules to be a heterogenous conglomeration of cells. The subcellular sites with the highest Brillouin shifts are predicted to be nuclei, based on a previous analysis of single cells.⁵⁴ Areas of Brillouin shifts as low as the liquid medium were observed within nodules, probably indicating regions with no cells and no matrix.

Penetration Depth of Brillouin Confocal Microscopy for Tumor Nodule Analysis

As with any optical technique, the penetration depth achieved by Brillouin microscopy in non-transparent samples is limited. Here, we analyzed the signal intensity as a function of depth for nodules on Matrigel and in low attachment cultures (Fig. 2c). We overlaid cells on Matrigel (Fig. 2a) and in 96 Well Ultra-Low Attachment Treated Spheroid Microplates which resulted in the formation of spheroids in suspension, without an exogenous extracellular matrix (Fig. 2b).⁴⁸ The sizes of nodules cultured using both techniques depend on culture time and seeding density. Previous work has shown that OVCAR5 cells overlaid on Matrigel form heterogenous nodules with a bimodal size distribution, which we observed as well.⁷ Consistent with the culture duration for mechanical testing, we analyzed Matrigel nodules on day 3 having a diameter of $\sim 50 \mu\text{m}$ and low attachment nodules on day 4 with a diameter of $\sim 850 \mu\text{m}$. As expected, the signal intensity of light through scattered medium decreased exponentially. The relationship between signal intensity (I) and depth (z) is commonly written as $I = I_0 e^{-\beta z}$ where I_0 is the incident light intensity and β is the scattering coefficient. In Fig. 2c, we show the natural log of the normalized intensity $\ln\left(\frac{I}{I_0}\right) = -\beta z$ and found the scattering coefficient β for low attachment nodules to be significantly greater than Matrigel nodules ($p \leq 0.0001$) (Fig. 2c).

To approximate the maximal penetration depth for Brillouin signal analysis, we assumed that a minimum of 3000 counts of incident light intensity is required. This condition equated to a maximum penetration

depth of $\sim 92 \mu\text{m}$ for Matrigel nodules and $\sim 54 \mu\text{m}$ for low attachment nodules. Additionally, we observed that increasing extracellular osmolality, using PBS with sucrose, decreased the signal penetration depth in both Matrigel and low attachment nodules. A penetration depth to enable Brillouin measurements was obtained for concentrations of sucrose of up to 1000 mM for Matrigel nodules and up to 125 mM for low attachment nodules.

Mechanical Behavior of Tumor Nodules Assessed Using Brillouin Confocal Microscopy

To alter the mechanical properties of the nodules, we immersed them in hyperosmotic solutions of PBS with up to 1000 mM of sucrose. We observed an increased Brillouin shift with increased osmolality of the solution in both Matrigel and low attachment nodules (Figs. 3a and 3b). The two methods, however, demonstrated similar trends in dependency between osmolality and Brillouin shift: Fig. 3c overlays both Figs. 3a and 3b measurements and shows a linear relationship between osmolality and Brillouin shift, independent of the nodule size and culture method.

Correlation of Mechanical Behavior of Tumor Nodules with AFM and MicroSquisher

To validate the ability of Brillouin Confocal Microscopy to analyze the mechanical properties of tumor nodules, we evaluated nodules undergoing similar osmotic changes using two standard approaches to extrapolate Young's modulus based on deformation of the sample: Atomic Force Microscopy and Micro-Scale Mechanical Tester (MicroSquisher). For these experiments, the nodules were cultured using the low attachment technique. Using AFM, (Fig. 4a) we found an increase in Young's modulus with increased osmolality (Fig. 4b). Similarly, using the MicroSquisher, (Fig. 4c) we found that the Young's modulus increased with increasing osmolality. The Young's modulus at 0–10% strain was evaluated and an exponential relationship ($R^2 = 0.95$) was found between Young's modulus and increasing osmolality (Fig. 4d). The averages and standard deviations for each condition are found in Table 3.

Carboplatin Decreases Brillouin Shift

Finally, we evaluated the mechanical effect of carboplatin treatment on 3D tumor nodules. Carboplatin is a commonly used anti-cancer chemotherapeutic to manage OvCa. We acquired brightfield images in the XY plane and Brillouin maps in the XZ plane. Compared to no treatment controls, nodules showed evi-

dence of morphological changes after carboplatin treatment (Fig. 5a). We also found carboplatin to cause a significant decrease in Brillouin shift ($p \leq 0.0001$) corresponding with a disrupted structure compared to the control group (Fig. 5b). These results were consistent with previous literature showing HeLa cells undergoing a significant decrease in stiffness and damaged morphology following treatment with paclitaxel.²³ More recently, Margueritat et al. used Brillouin Confocal Microscopy to quantify tumor mechanics post chemotherapy and showed the tumor core had decreased drug efficacy.²⁶ Since OVCAR5 cells cultured on Matrigel form 3D nodules with a bimodal size distribution,⁷ the relationships between tumor size, treatment response and mechanical properties will be important to investigate in future studies. In addition, the possibility that drug resistant tumor cell populations have a decreased stiffness due to a more metastatic behavior should not be ruled out and would be an interesting experiment for the future.

DISCUSSION

The mechanical properties of cells and extracellular components play critical roles in cell behaviors such as migration, differentiation, proliferation, and survival.^{12,18,24,30,52} The need for technologies to quantify mechanical properties on a cellular level is widely recognized; thus, in the past two decades, tools including AFM, micropipette aspiration, optical stretchers, microfluidics, and microrheology have been developed.^{2,14,16,27,50} Despite each of their strengths, analysis of 3D in vitro cultures, which are increasingly prevalent, requires destruction of the sample. AFM and micropipette aspiration both require direct contact with the sample, thus preventing the analysis of experiments involving nodules encapsulated in 3D microenvironments or within microfluidic devices.^{14,50} Both optical stretchers and microfluidic channels have enhanced the ability for high throughput mechanical analysis but they require deformation of the sample.^{14,16,50} Microrheology is useful for assessing the effects in 3D microenvironments; however, this technique is still invasive and involves tracing microparticles undergoing Brownian motion, so the data output typically involves trajectories of paths rather than mapping of the entire cell structure.^{27,50}

Brillouin Confocal Microscopy is an all-optical method that can resolve mechanical information in 3D in vitro cultures without contact and with micron scale resolution. However, Brillouin does not provide information for traditional metrics such as Young's modulus. Thus, to align with gold standard technologies, we performed a validation to study the mechan-

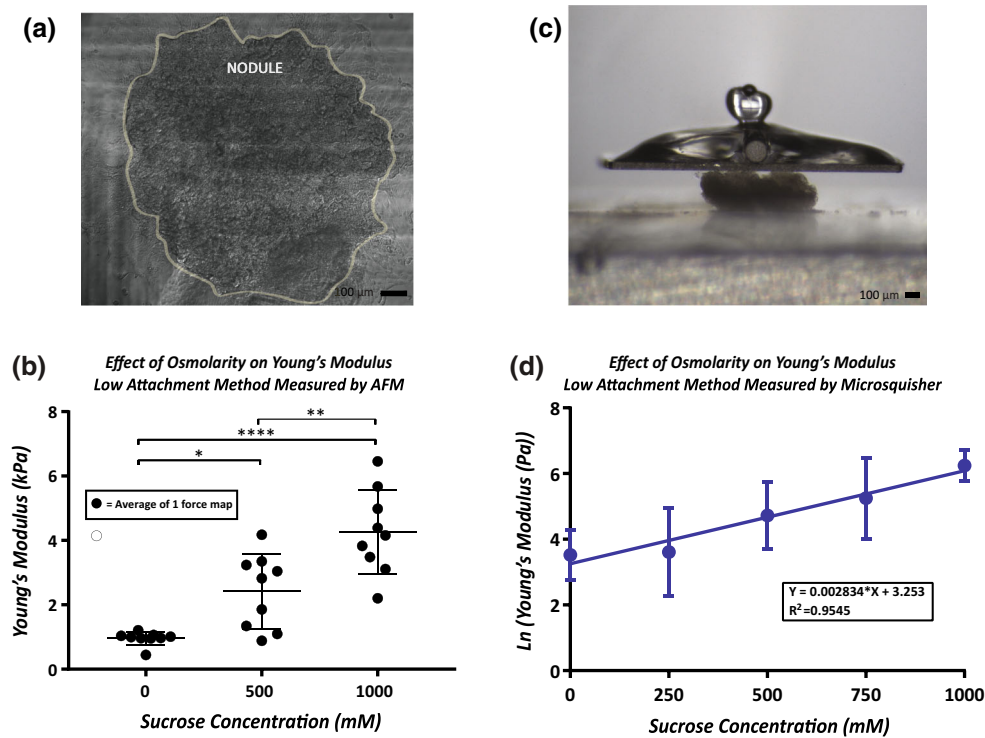


FIGURE 4. (a) Example of nodule attached to collagen coated measured by AFM. Three force maps per nodule spanning an area of $2500 \mu\text{m}^2$ each were measured. (b) Increased osmolality caused an increased Young's modulus measured by AFM. (c) Example of nodule being contacted by Microsquisher parallel compression plate. (d) Increased osmolality exhibited an exponential relationship with Young's modulus measured by the Microsquisher.

TABLE 3. Results summary for mechanical testing of nodules under varying sucrose concentrations.

Results summary			
Technique	Culture method	Sucrose (mM)	Mean \pm standard deviation
Brillouin	Matrigel	0	6.33 ± 0.03 GHz
		500	6.67 ± 0.07 GHz
		1000	6.93 ± 0.07 GHz
Brillouin	Low Attachment	0	6.32 ± 0.04 GHz
		62.5	6.37 ± 0.02 GHz
		125	6.42 ± 0.03 GHz
AFM	Low Attachment	0	0.96 ± 0.18 kPa
		500	2.42 ± 1.09 kPa
		1000	4.25 ± 1.23 kPa
Microsquisher	Low Attachment	0	42.32 ± 26.69 Pa
		250	86.35 ± 140.13 Pa
		500	168.47 ± 156.81 Pa
		750	329.12 ± 314.43 Pa
		1000	562.09 ± 246.82 Pa

ical properties of ovarian cancer nodules. We evaluated two different culture techniques since each showed benefits contingent on the mechanical analysis technology. We observed Brillouin to be advantageous compared to AFM and the MicroSquisher in measuring 3D tumor nodules in overlay cultures on Matrigel. AFM analysis of nodules cultured using

Matrigel posed challenges due to the interference of the gel with the probe and forces felt beneath the nodule caused by the low Young's modulus of Matrigel. To isolate adherent 3D nodules from the underlying Matrigel matrix, centrifugation and enzymatic methods have been used, but these methods are highly disruptive to the nodules. Culturing on Matrigel was also

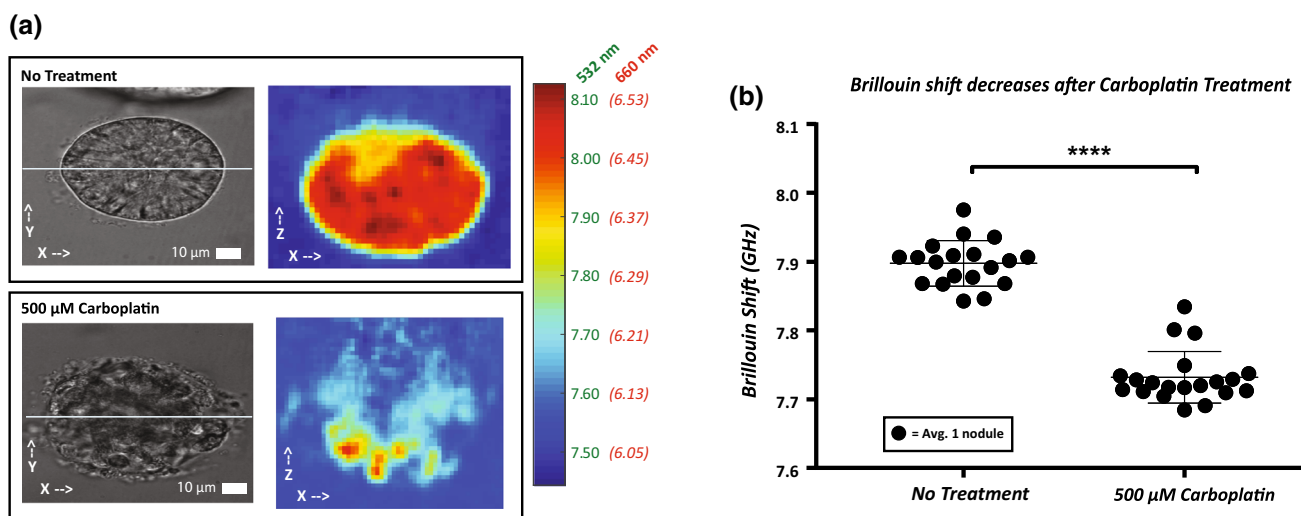


FIGURE 5. (a) Brightfield images and corresponding Brillouin maps of no treatment and carboplatin treated nodules. Color bar represents Brillouin shift (GHz) represented in both 660 nm and 532 nm incident wavelengths. (b). Brillouin Shift of no treatment 500 μM carboplatin measured using Brillouin. A threshold of 7.65 GHz was used to isolate nodules from surrounding medium. The Brillouin shift was significantly lower in the 500 μM carboplatin group compared to no treatment group ($p \leq 0.0001$).

unfavorable for MicroSquisher analysis which requires samples to be greater than 50 μm and attached to a hard surface. Of the two culture techniques, we found the low attachment method to be better suited for AFM and the MicroSquisher. On the other hand, Brillouin had challenges in imaging nodules generated by the protocol used here for low attachment cultures due to the large size and opacity of the spheroids. In the future, a lower initial seeding density could be used to form smaller nodules and ensure whole nodule measurements with Brillouin. Consequentially, the low penetration depth of Brillouin signal may limit applications to cancer bio-mechanics studies. For instance, hypoxic cores are introduced in nodules greater than 200 μm .⁹ Whereas, our findings show the maximum penetration depth of Brillouin signal is $\sim 92 \mu\text{m}$ for Matrigel nodules and $\sim 54 \mu\text{m}$ for low attachment nodules. Additionally, extracting mechanical properties from real tissue specimens may better mimic the in vivo mechanical state due to the extracellular matrix and tumor cell heterogeneity. However, opacity and size of a biopsy sample may inhibit such measurements. Accordingly, until further advances are made in the Brillouin technology, experimental designs must be coordinated with the current specifications.

Both protocols appear to be uniquely advantageous; for example, Matrigel can vary batch-to-batch thus producing variable results; yet, depending on the cell line, the method yields a collection of heterogenous tumors in the same well, so mechanics in conjunction with migration and proliferation can be determined.⁷ Finally, it is important to acknowledge the differences in sampling resolutions for each of the three systems used to assess the mechanical properties of the 3D

tumor nodules. Brillouin can create maps of the entire nodule in three axes, although here we reduced the maps to one average value for comparison. AFM can generate a map with micron resolution as well, but only in one axis while the Microsquisher only generates a single value per sample. Thus, the optimal technology choice is dependent on both culture technique and sampling interests.

As shown in this work, the mechanical measurements in 3D tumor nodules performed by Brillouin microscopy correlate with the gold standard mechanical measurements. Using AFM, we found that OVCAR5 nodules had an average Young's modulus of 0.96 kPa in PBS. Because the tip of the AFM probe was approximately 5 μm , the Young's modulus of a nodule was resolvable to the level of single cells. A similar range of Young's moduli have been previously reported for other ovarian cancer cell lines: OVCAR4: 1.120 kPa, HEY: 0.884 kPa, OVCAR3: 0.576 kPa, and HEYA8: 0.494 kPa.⁵² In comparison, non-malignant immortalized ovarian surface epithelial cells had a Young's modulus of 2.472 kPa.⁵² Using the MicroSquisher, we found that OVCAR5 nodules had an average Young's modulus of 42.32 Pa in PBS and an exponential correlation was observed with increasing sucrose concentration. The Young's modulus of spheroids composed of mesenchymal stem cells was previously measured using the MicroSquisher and was found to be on a similar scale of $42.28 \pm 6.14 \text{ Pa}$ at 20% strain.⁵

In the present study, Brillouin shift evaluated optically, and Young's modulus determined by AFM and Microsquisher, all increased with increasing osmolality. Previous reports measuring single cells subjected to

hyperosmolar conditions provided similar results.^{17,40,55} It is believed that increasing osmolality causes water efflux from cells, reduction of cell volume, and crowding of the intracellular space. In our experiments, a reduction in tumor volume was visible immediately following sucrose addition.^{17,55} The relationship between cell volume and cell stiffness has spawned further questions on how cells regulate volume and behavioral consequences. Guo *et al.* recently showed that changes in cell volume, due to either osmotic stress or matrix stiffness, influenced stem cell differentiation.¹⁷ The consequences of cell volume changes in cancer cells is less understood but may be highly relevant in tumorigenesis, where cancer cells experience a variety of external physical forces.^{6,29}

A critical next step is to identify Brillouin sensitivity to changes in cell stiffness due to different phenomena, such as solid/liquid fraction changes, variation in cell contractility, crowding of intracellular space, or cytoskeletal polymerization/crosslinking. Recent work revealed that at high water content (> 95%), Brillouin measurements are strongly affected by water content compared to traditional mechanical testing systems to the point of practically being unable to characterize mechanical effects in highly hydrated gels.^{37,51} However, in single cells and tissues, which have approximately ~ 70% water content, Brillouin shift and Young's modulus have both been shown to be sensitive to water content.^{21,40} Thus, a strong correlation between Brillouin microscopy and traditional mechanical testing is generally observed and Brillouin technology appears to be sensitive to several relevant phenomena such as collagen crosslinking/branching,³⁹ chromatin decondensation⁵⁴ and activation/inhibition of actin polymerization.⁴⁰

CONCLUSION

In summary, we developed and validated a novel application of Brillouin Confocal Microscopy to evaluate the mechanical properties of 3D cancer nodules grown in suspension using ultra-low attachment plates and in adherent overlay cultures on Matrigel. In response to osmotic pressure changes, we found that 3D nodules demonstrated increased Brillouin shift measured by Brillouin microscopy, which corresponded with increased Young's modulus measured using both AFM and the MicroSquisher. We expect that this increase in stiffness is due to an increase in the extracellular sucrose concentration causing efflux of water from cells, resulting in intracellular compression. Furthermore, we showed that carboplatin treatment at 500 μ M caused a significant decrease in Brillouin shift in 3D nodules within the size range measured here,

which appeared to correlate with a loss of structural integrity of nodules. In the long term, we plan to harness the advantages of an all-optical technology to evaluate the mechanical effects of tumor nodules in response to phenomena relevant to disease pathology such as fluid stress and 3D microenvironments in ovarian cancer.

FUNDING

This work is supported in part by the National Institutes of Health (R00 CA175292, R33CA204582 and U01CA202177), National Science Foundation (CMMI-1537027). The authors also acknowledge funding from the Burroughs Wellcome Career Award at the Scientific Interface (to KMS).

CONFLICT OF INTEREST

The authors, Christina Conrad, Kelsey M. Gray, Kimberly M. Stroka, Imran Rizvi, and Giuliano Scarcelli declare that they have no conflict of interest.

ETHICAL APPROVAL

No animal or human studies were carried out by the authors for this article.

REFERENCES

- ¹Ahmed, N., K. Abubaker, J. Findlay, and M. Quinn. Epithelial Mesenchymal Transition and Cancer Stem Cell-Like Phenotypes Facilitate Chemoresistance in Recurrent Ovarian Cancer. *Curr. Cancer Drug Targets*. 10:268–278, 2010.
- ²Alibert, C., B. Goud, and J. B. Manneville. Are cancer cells really softer than normal cells? *Biol Cell*. 109:167–189, 2017.
- ³Baker, B. M., and C. S. Chen. Deconstructing the third dimension—how 3D culture microenvironments alter cellular cues. *J. Cell Sci*. 125:3015–3024, 2012.
- ⁴Bankhead, C. R., C. Collins, H. Stokes-Lampard, P. Rose, S. Wilson, A. Clements, D. Mant, S. T. Kehoe, and J. Austoker. Identifying symptoms of ovarian cancer: a qualitative and quantitative study. *BJOG* 115:1008–1014, 2008.
- ⁵Baraniak, P. R., M. T. Cooke, R. Saeed, M. A. Kinney, K. M. Fridley, and T. C. McDevitt. Stiffening of human mesenchymal stem cell spheroid microenvironments induced by incorporation of gelatin microparticles. *J. Mech. Behav. Biomed. Mater.* 11:63–71, 2012.
- ⁶Butcher, D. T., T. Alliston, and V. M. Weaver. A tense situation: forcing tumour progression. *Nat. Rev. Cancer* 9:108–122, 2009.

- ⁷Celli, J. P., I. Rizvi, C. L. Evans, A. O. Abu-Yousif, and T. Hasan. Quantitative imaging reveals heterogeneous growth dynamics and treatment-dependent residual tumor distributions in a three-dimensional ovarian cancer model. *J. Biomed. Opt.* 15:51603, 2010.
- ⁸Cress, R. D., Y. S. Chen, C. R. Morris, M. Petersen, and G. S. Leiserowitz. Characteristics of long-term survivors of epithelial ovarian cancer. *Obstet. Gynecol.* 126:491–497, 2015.
- ⁹Däster, S., N. Amatruda, D. Calabrese, R. Ivanek, E. Turrini, R. A. Droeser, P. Zajac, C. Fimognari, G. C. Spagnoli, G. Iezzi, V. Mele, and M. G. Muraro. Induction of hypoxia and necrosis in multicellular tumor spheroids is associated with resistance to chemotherapy treatment. *Oncotarget* 8:1725–1736, 2016.
- ¹⁰de Sousa, G. F., S. R. Wlodarczyk, and G. Monteiro. Carboplatin: molecular mechanisms of action associated with chemoresistance. *Braz. J. Pharm. Sci.* 50:693–701, 2014.
- ¹¹Dong, C., X. Hu, and C. Z. Dinu. Current status and perspectives in atomic force microscopy-based identification of cellular transformation. *Int. J. Nanomed.* 11:2107–2118, 2016.
- ¹²Engler, A. J., S. Sen, H. L. Sweeney, and D. E. Discher. Matrix elasticity directs stem cell lineage specification. *Cell* 126:677–689, 2006.
- ¹³Gajjar, K., G. Ogden, M. I. Mujahid, and K. Razvi. Symptoms and risk factors of ovarian cancer: a survey in primary care. *ISRN Obstet. Gynecol.* 2012. <https://doi.org/10.5402/2012/754197>.
- ¹⁴Gossett, D. R., H. T. K. Tse, S. A. Lee, Y. Ying, A. G. Lindgren, O. O. Yang, J. Rao, A. T. Clark, and D. Di Carlo. Hydrodynamic stretching of single cells for large population mechanical phenotyping. *PNAS* 109:7630–7635, 2012.
- ¹⁵Griffith, L. G., and M. A. Swartz. Capturing complex 3D tissue physiology in vitro. *Nat. Rev. Mol. Cell Biol.* 7:211, 2006.
- ¹⁶Guck, J., R. Ananthakrishnan, T. J. Moon, C. C. Cunningham, and J. Kas. Optical deformability of soft biological dielectrics. *Phys. Rev. Lett.* 84:5451–5454, 2000.
- ¹⁷Guo, M., A. F. Pegoraro, A. Mao, E. H. Zhou, P. R. Arany, Y. Han, D. T. Burnette, M. H. Jensen, K. E. Kasza, J. R. Moore, F. C. Mackintosh, J. J. Fredberg, D. J. Mooney, J. Lippincott-Schwartz, and D. A. Weitz. Cell volume change through water efflux impacts cell stiffness and stem cell fate. *PNAS* 114:E8618–E8627, 2017.
- ¹⁸Hyer, A. R., N. C. Baudoin, M. S. Brown, M. A. Stremler, D. Cimini, R. V. Davalos, and E. M. Schmelz. Fluid shear stress impacts ovarian cancer cell viability, subcellular organization, and promotes genomic instability. *PLoS ONE* 13:e0194170, 2018.
- ¹⁹Ingber, D. E. Cellular mechanotransduction: putting all the pieces together again. *FASEB J.* 20:811–827, 2006.
- ²⁰Iwatsuki, M., K. Mimori, T. Yokobori, H. Ishi, T. Beppu, S. Nakamori, H. Baba, and M. Mori. Epithelial-mesenchymal transition in cancer development and its clinical significance. *Cancer Sci.* 101:293–299, 2010.
- ²¹Kageyama, K., Y. Onoyama, H. Kogawa, E. Goto, and K. Tanabe. The maximum and minimum water content and cell volume of human erythrocytes in vitro. *Biophys. Chem.* 34:79–82, 1989.
- ²²Ketene, A. N., E. M. Schmelz, P. C. Roberts, and M. Agah. The effects of cancer progression on the viscoelasticity of ovarian cell cytoskeleton structures. *Nanomedicine.* 8:93–102, 2012.
- ²³Kim, K. S., C. H. Cho, E. K. Park, M.-H. Jung, K.-S. Yoon, and H.-K. Park. AFM-detected apoptotic changes in morphology and biophysical property caused by Paclitaxel in Ishikawa and HeLa Cells. *PLoS ONE* 7:e30066, 2012.
- ²⁴Kumar, S., and V. M. Weaver. Mechanics, malignancy, and metastasis: the force journey of a tumor cell. *Cancer Metastasis Rev.* 28:113–127, 2009.
- ²⁵Labidi-Galy, S. I., et al. High grade serous ovarian carcinomas originate in the fallopian tube. *Nat. Commun.* 8:1093, 2017.
- ²⁶Margueritat, J., A. Virgone-Carlotta, S. Monnier, H. Delanoë-Ayari, H. C. Mertani, A. Berthelot, Q. Martinet, X. Dagany, C. Rivière, J.-P. Rieu, and T. Dehoux. High-frequency mechanical properties of tumors measured by Brillouin light scattering. *Phys. Rev. Lett.* 122:018101, 2019.
- ²⁷Mason, T. G., and D. A. Weitz. Optical measurements of frequency-dependent linear viscoelastic moduli of complex fluids. *Phys. Rev. Lett.* 74:1250–1253, 2018.
- ²⁸McGrail, D. J., Q. M. N. Kieu, and M. R. Dawson. The malignancy of metastatic ovarian cancer cells is increased on soft matrices through a mechanosensitive Rho–ROCK pathway. *J. Cell Sci.* 127:2621–2626, 2014.
- ²⁹McGrail, D. J., K. M. McAndrews, C. P. Brandenburg, N. Ravikumar, Q. M. Kieu, and M. R. Dawson. Osmotic regulation is required for cancer cell survival under solid stress. *Biophys. J.* 109:1334–1337, 2015.
- ³⁰McKenzie, A. J., S. R. Hicks, K. V. Svec, H. Naughton, Z. L. Edmunds, and A. K. Howe. The mechanical microenvironment regulates ovarian cancer cell morphology, migration, and spheroid disaggregation. *Sci. Rep.* 8:7228, 2018.
- ³¹Moeendarbary, E., L. Valon, M. Fritzsche, A. R. Harris, D. A. Moulding, A. J. Thrasher, E. Stride, L. Mahadevan, and G. T. Charras. The cytoplasm of living cells behaves as a poroelastic material. *Nat. Mater.* 12:253, 2013.
- ³²Novak, C., E. Horst, and G. Mehta. Review: mechanotransduction in ovarian cancer: shearing into the unknown. *APL Bioeng.* 2:31701, 2018.
- ³³Polacheck, W. J., A. E. German, A. Mammoto, D. E. Ingber, and R. D. Kamm. Mechanotransduction of fluid stresses governs 3D cell migration. *Proc. Natl. Acad. Sci. U.S.A.* 111:2447–2452, 2014.
- ³⁴Polacheck, W. J., M. L. Kutys, J. Yang, J. Eyckmans, Y. Wu, H. Vasavada, K. K. Hirschi, and C. S. Chen. A non-canonical Notch complex regulates adherens junctions and vascular barrier function. *Nature* 552:258, 2017.
- ³⁵Reid, B. M., J. B. Permeth, and T. A. Sellers. Epidemiology of ovarian cancer: a review. *Cancer Biol. Med.* 14:9–32, 2017.
- ³⁶Rizvi, I., U. A. Gurkan, S. Tasoglu, N. Alagic, J. P. Celli, L. B. Mensah, Z. Mai, U. Demirci, and T. Hasan. Flow induces epithelial-mesenchymal transition, cellular heterogeneity and biomarker modulation in 3D ovarian cancer nodules. *PNAS* 110:1974–1983, 2013.
- ³⁷Scarcelli, G., and S. H. Yun. Reply to ‘Water content, not stiffness, dominates Brillouin spectroscopy measurements in hydrated materials’. *Nat. Methods* 15:561–565, 2018.
- ³⁸Scarcelli, G., P. Kim, and S. H. Yun. In vivo measurement of age-related stiffening in the crystalline lens by Brillouin optical microscopy. *Biophys. J.* 101:1539–1545, 2011.

- ³⁹Scarcelli, G., S. Kling, E. Quijano, R. Pineda, S. Marcos, and S. H. Yun. Brillouin microscopy of collagen crosslinking: noncontact depth-dependent analysis of corneal elastic modulus. *Invest. Ophthalmol. Vis. Sci.* 54:1418–1425, 2013.
- ⁴⁰Scarcelli, G., W. J. Polacheck, H. T. Nia, K. Patel, A. J. Grodzinsky, R. D. Kamm, and S. H. Yun. Noncontact three-dimensional mapping of intracellular hydro-mechanical properties by Brillouin microscopy. *Nat. Methods* 12:1132–1134, 2015.
- ⁴¹Schindelin, J., I. Arganda-Carreras, E. Frise, V. Kaynig, M. Longair, T. Pietzsch, S. Preibisch, C. Rueden, S. Saalfeld, B. Schmid, J.-Y. Tinevez, D. J. White, V. Hartenstein, K. Eliceiri, P. Tomancak, and A. Cardona. Fiji: an open-source platform for biological-image analysis. *Nat. Methods* 9:676, 2012.
- ⁴²Shao, P., T. G. Seiler, A. M. Eltony, A. Ramier, S. J. J. Kwok, G. Scarcelli, R. P. Ii, and S.-H. Yun. Effects of corneal hydration on Brillouin microscopy in vivo. *Invest. Ophthalmol. Vis. Sci.* 59:3020–3027, 2018.
- ⁴³Siegel, R. L., K. D. Miller, and A. Jemal. Cancer statistics, 2017. *CA. Cancer J. Clin.* 67:7–30, 2017.
- ⁴⁴Swaminathan, V., K. Mythreye, E. T. O'Brien, A. Berchuck, G. C. Blobe, and R. Superfine. Mechanical stiffness grades metastatic potential in patient tumor cells and in cancer cell lines. *Cancer Res.* 71:5075–5080, 2011.
- ⁴⁵Swartz, M. A., N. Iida, E. W. Roberts, S. Sangaletti, M. H. Wong, F. E. Yull, L. M. Coussens, and Y. A. DeClerck. Tumor microenvironment complexity: emerging roles in cancer therapy. *Cancer Res.* 72:2473–2480, 2012.
- ⁴⁶Tan, D. S., R. Agarwal, and S. B. Kaye. Mechanisms of transcoelomic metastasis in ovarian cancer. *Lancet Oncol.* 7:925–934, 2006.
- ⁴⁷Webb, J. N., J. P. Su, and G. Scarcelli. Mechanical outcome of accelerated corneal crosslinking evaluated by Brillouin microscopy. *J. Cataract Refract. Surg.* 43:1458–1463, 2017.
- ⁴⁸Weiswald, L. B., D. Bellet, and V. Dangles-Marie. Spherical cancer models in tumor biology. *Neoplasia* 17:1–15, 2015.
- ⁴⁹Wirtz, D., K. Konstantopoulos, and P. C. Searson. The physics of cancer: the role of physical interactions and mechanical forces in metastasis. *Nat. Rev. Cancer* 11:512, 2011.
- ⁵⁰Wu, P.-H., *et al.* A comparison of methods to assess cell mechanical properties. *Nat. Methods* 15:491, 2018.
- ⁵¹Wu, P.-J., I. V. Kabakova, J. W. Ruberti, J. M. Sherwood, I. E. Dunlop, C. Paterson, P. Török, and D. R. Overby. Water content, not stiffness, dominates Brillouin spectroscopy measurements in hydrated materials. *Nat. Methods* 15:561, 2018.
- ⁵²Xu, W., R. Mezecevic, B. Kim, L. Wang, J. McDonald, and T. Sulchek. Cell stiffness is a biomarker of the metastatic potential of ovarian cancer cells. *PLoS ONE* 7:e46609, 2012.
- ⁵³Zaman, M. H., L. M. Trapani, A. L. Sieminski, D. MacKellar, H. Gong, R. D. Kamm, A. Wells, D. A. Lauffenburger, and P. Matsudaira. Migration of tumor cells in 3D matrices is governed by matrix stiffness along with cell-matrix adhesion and proteolysis. *Proc. Natl. Acad. Sci. U.S.A.* 103:10889–10894, 2006.
- ⁵⁴Zhang, J., X. A. Nou, H. Kim, and G. Scarcelli. Brillouin flow cytometry for label-free mechanical phenotyping of the nucleus. *Lab Chip* 17:663–670, 2017.
- ⁵⁵Zhou, E. H., X. Trepat, C. Y. Park, G. Lenormand, M. N. Oliver, S. M. Mijailovich, C. Hardin, D. A. Weitz, J. P. Butler, and J. J. Fredberg. Universal behavior of the osmotically compressed cell and its analogy to the colloidal glass transition. *PNAS.* 106:10632–10637, 2009.

Publisher's Note Springer Nature remains neutral with regard to jurisdictional claims in published maps and institutional affiliations.